

## Smoke-impacted regional haze in California during the summer of 2002

Gavin R. McMeeking<sup>a</sup>, Sonia M. Kreidenweis<sup>a,\*</sup>, Melissa Lunden<sup>b</sup>,  
Jacqueline Carrillo<sup>a</sup>, Christian M. Carrico<sup>a</sup>, Taehyoung Lee<sup>a</sup>, Pierre Herckes<sup>a,1</sup>,  
Guenter Engling<sup>a</sup>, Derek E. Day<sup>c</sup>, Jennifer Hand<sup>c</sup>, Nancy Brown<sup>b</sup>,  
William C. Malm<sup>c</sup>, Jeffrey L. Collett Jr.<sup>a</sup>

<sup>a</sup>Department of Atmospheric Science, Colorado State University, Fort Collins, CO 80523, USA

<sup>b</sup>Lawrence Berkeley Laboratory, 1 Cyclotron Road, MS 51R0208, Berkeley, CA 94720, USA

<sup>c</sup>Cooperative Institute for Research in the Atmosphere (CIARA), Colorado State University, Fort Collins, CO 80523, USA

Received 26 September 2005; accepted 17 January 2006

### Abstract

Observations of aerosol physical, chemical, and optical properties made at 38 locations in Washington, Oregon, and California are presented to show the regional-scale influence of wildfire smoke during the summer of 2002. Aerosol measurements made during an intensive field campaign conducted in July, August, and September 2002 in Yosemite National Park indicated that smoke-impacted aerosols were present at the park during frequent haze episodes. In addition, backward trajectory analyses showed that large-scale meteorological conditions during the study were dominated by transport from western and southern Oregon, a region with high fire activity during the summer of 2002. Observations of aerosol properties at the Yosemite NP site were remarkably similar, with similar temporal variations, to data from a second monitoring site at Blodgett Forest Research Station in the Sierra Nevada, approximately 150 km to the NNW. Further similarities to the temporal changes in aerosol properties as measured by monitoring networks with numerous sites in California and Oregon confirmed the regional nature of the haze, which had elevated fine aerosol particle mass concentrations compared with typical summertime average concentrations. The observations suggest that emissions from wild fires can have strong and sustained regional impacts on aerosol concentrations, air quality, and visibility. © 2006 Elsevier B.V. All rights reserved.

**Keywords:** Aerosol; Smoke; Regional scale; Haze; Carbon; Wildland fire

### 1. Introduction

Aerosol particles play important roles in atmospheric chemical cycles, in visibility degradation, and in the Earth's radiative balance. Although ionic species are often major components of the atmospheric aerosol,

recent observations have shown that carbonaceous compounds are ubiquitous and sometimes dominate the submicron aerosol mass (Malm et al., 2004; Putaud et al., 2004; Saxena and Hildemann, 1996; Rogge et al., 1993; Bevington and Robinson, 1992; Andreae, 1983). In some regions and seasons, biomass burning can be the major source of particulate matter, and carbonaceous aerosols are the single largest component of biomass burning aerosols (Formenti et al., 2003; Cachier et al., 1995; Artaxo et al., 1988; Andreae, 1983). Bond et al. (2004) estimate the relative contributions of fossil fuel, biofuel, and open burning

\* Corresponding author. Tel.: +1 970 491 8350; fax: +1 970 491 8483.

E-mail address: [sonia@atmos.colostate.edu](mailto:sonia@atmos.colostate.edu) (S.M. Kreidenweis).

<sup>1</sup> Present address: Department of Chemistry and Biochemistry, Arizona State University, Tempe, AZ, United States.

to global combustion-derived organic carbon emissions as 7%, 19%, and 74%, respectively. Niemi et al. (2005) showed that elevated aerosol concentration episodes in Finland were due in part to transport from fire emissions in Russia and eastern Europe. In the western United States, forest fires have been shown to contribute to elevated aerosol organic carbon (OC) and light-absorbing carbon (LAC) concentrations, which are in turn associated with decreased visibility (Ames et al., 2004; Malm et al., 2004).

An improved understanding of the role of fire emissions, from controlled burns as well as from wildfires, is an important component of strategies for compliance with the Regional Haze Rule (<http://www.epa.gov/oar/visibility/program.html>), especially in the western U.S. (Watson, 2002). As United States fire management policies evolve, it is necessary to consider the consequences of increased amounts of controlled burning on air quality and visibility in protected areas. Further, accurate estimates of the regional effects of emissions from wildfires are required to determine the contributions of wildfires to natural visibility conditions, a benchmark for measuring progress under the Regional Haze Rule.

To illustrate typical levels of and seasonal variations in carbonaceous aerosols in the western U.S., Fig. 1 shows organic mass concentrations in fine particulate matter measured for the period 1988–2004 at a representative western site, Yosemite National Park (YNP), California. The data were obtained from the Interagency Monitoring of Protected Visual Environments (IMPROVE) network database. Organic mass was calculated by multiplying measured organic carbon concentrations by a factor of 1.8, which Malm et al.

(2005) showed gave good agreement between reconstructed and measured fine particle mass at the park during the study. Averaged organic mass concentrations are lowest during the winter and spring months, reaching higher concentrations during the late summer and early fall. This seasonality is reflected in most forested, temperate sites in the network (Ames et al., 2004; Malm et al., 2004), and can be attributed to increased emissions of biogenic aerosol precursors during the summertime and enhanced photochemistry that is a key factor in the generation of secondary organic aerosols (SOA). Fig. 1 also shows that the monthly variability of organic aerosol mass concentrations is much lower during the winter and spring than for the summer and fall seasons. The higher variability seen during the summer months, and the extreme concentrations observed in certain years, are likely due to wildfire activity, itself highly variable from year to year as well as within each fire season.

The Yosemite Aerosol Characterization Study was conducted in summer 2002 in YNP to provide a better description of the relative roles of wildfire, biogenic, and anthropogenic emissions in summertime visibility degradation in the western United States. Fig. 1 shows that OC concentrations during 2002 were similar to previous years. The study was focused on obtaining detailed measurements of the physical, chemical, and optical properties of carbonaceous aerosols (Carrico et al., 2005; Engling et al., 2005; Hand et al., 2005; Malm et al., 2005; McMeeking et al., 2005a,b; Bench and Herckes, 2004). During the same period, intensive aerosol measurements were also made at another site in the western Sierra Nevada near the University of California Blodgett Forest Research Station (BFRS).

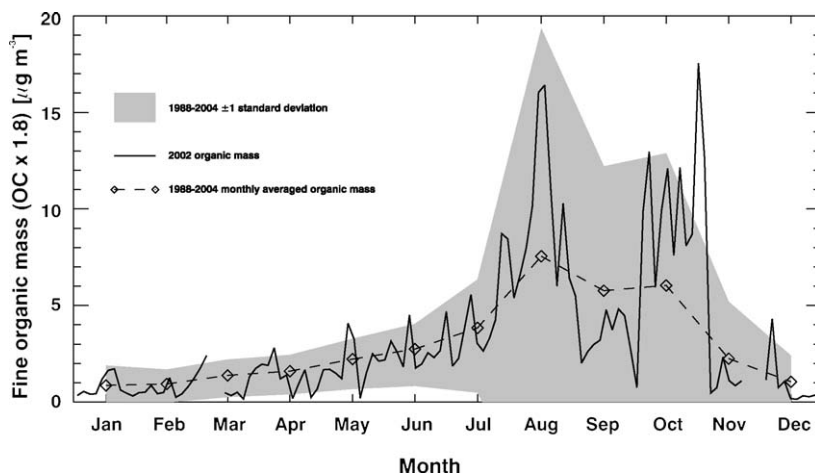


Fig. 1. Monthly averaged  $PM_{2.5}$  organic mass (organic carbon  $\times$  1.8) concentrations and standard deviations for the time period 1988–2004 and concentrations for 2002 measured at the Turtleback Dome IMPROVE site in Yosemite National Park.

Although BFRS is located approximately 150 km NNW of YNP, the aerosol data from the two sites show remarkable coherence in both the magnitudes of the measured properties and in their temporal variability, suggesting the haze was present on a large, i.e. regional scale. Several massive wild fires were active in California and Oregon during the study. We use meteorological and in situ aerosol and optical data to demonstrate that emissions from these fires contributed to haze observed not only in the Sierra Nevada, but on a scale encompassing a large area of Oregon and California.

## 2. Methods

### 2.1. Aerosol measurement sites and data

The data presented in this paper were collected at 38 sites from 15 July to 5 September 2002 (Fig. 2). These locations include high time resolution data collected during two different intensive summer aerosol sampling studies located in YNP and BFRS, routine aerosol and visibility data from the IMPROVE network, and aerosol properties calculated from cloud-screened level 2.0 sun photometer data from the Aerosol Robotic

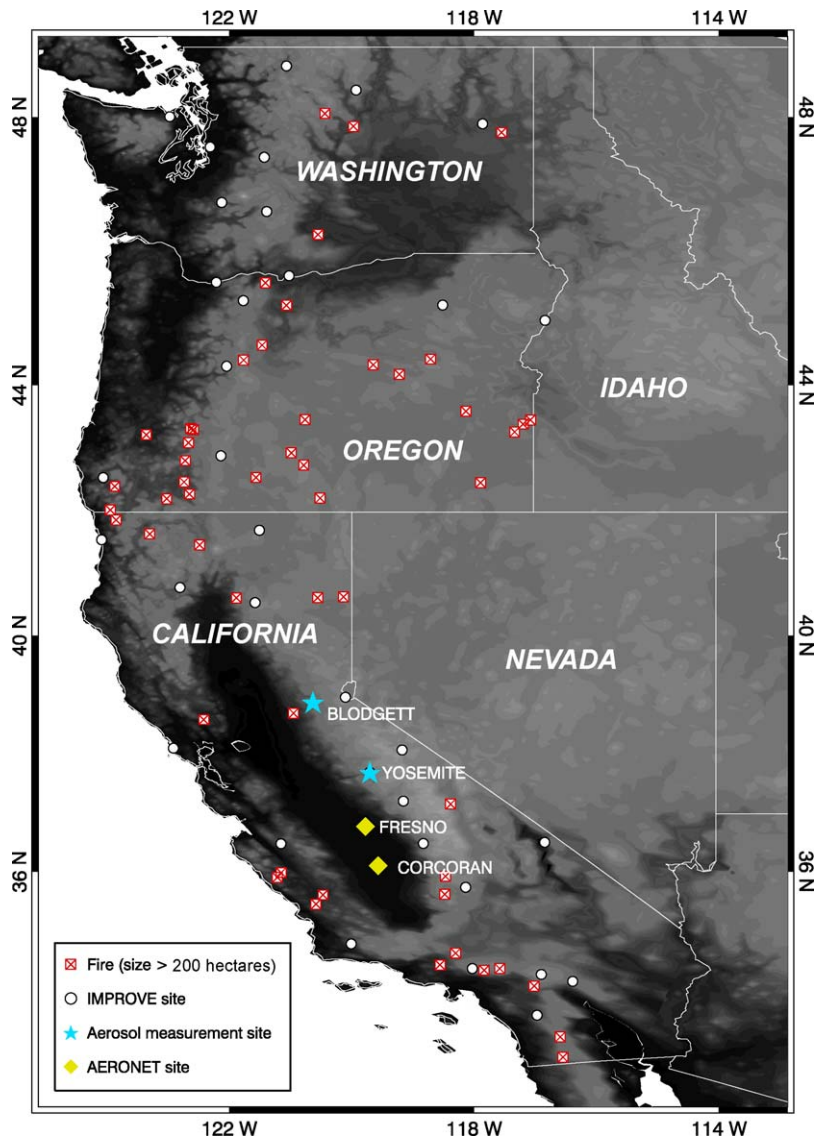


Fig. 2. Locations of the Turtleback Dome (Yosemite NP), Blodgett Forest, AERONET, and IMPROVE measurement sites. The locations of wildfires greater than 200 ha in size as reported by the National Interagency Fire Center (NIFC) occurring in Washington, Oregon, and California during the period 10 July 2002–5 September 2002 are also shown. Particularly large fires occurred on the western side of the Oregon–California border (Biscuit Fire) and just east of Corcoran, CA near Sequoia NP (McNally Fire).

Table 1  
Summary of aerosol measurements and instrumentation

Measurement	Turtleback Dome, Yosemite	Blodgett Forest	IMPROVE	Fresno	Corcoran	2.5 $\mu\text{m}$ cutpoint?
Light absorbing carbon	2-Channel aethalometer ( <i>0.1</i> )	2-Channel aethalometer	Thermal optical reflectance (TOR) method ( <i>0.072</i> )	–	–	No
Potassium (ion for URG measurement)	URG ( <i>0.005</i> ), IMPROVE	–	PIXE elemental analysis ( <i>0.0004</i> )	–	–	Yes
Organic carbon	TOR OC/EC ( <i>0.33</i> )	–	TOR EC/OC ( <i>0.33</i> )	–	–	Yes
Size distributions	DMPS, OPC (38 nm–3 $\mu\text{m}$ )	DMPS (10–400 nm)	–	AERONET sun photometer	AERONET sun photometer	–
Aerosol light scattering ( $b_{\text{sp}}$ )	Nephelometer (Optec NGN-2 ambient)	Nephelometer (Optec NGN-2 ambient)	–	Nephelometer	–	No

Levels of detection are given in italic for selected measurements in  $\mu\text{g m}^{-3}$ . IMPROVE levels of detection are taken from the average minimum detection limit (MDL) reported by IMPROVE during the study. The URG MDL is given by Lee (personal communication). Aethalometer detection limit is given by the instrument website (<http://www.mageesci.com>; Magee Scientific, Berkeley, California).

Network (AERONET) (Holben et al., 1998). Detailed descriptions of the measurements, including data quality assurance and quality control, are given in references cited for each measurement below. Here we provide a brief description of each measurement. Table 1 shows the aerosol characterization measurements collected at each location that will be discussed in this work. The measurement sites and instruments are described in the same order as in the table: Turtleback Dome, Yosemite, Blodgett Forest, IMPROVE, Fresno, and Corcoran.

Detailed measurements of aerosol optical, chemical, and physical properties were made at Turtleback Dome, Yosemite (37.71°N, 119.7°W, 1615 m elevation) in YNP, which is an elevated site located at the western end of Yosemite Valley. The park is located approximately 200 km east of San Francisco, California. High-volume filter measurements were made in the same area as the standard IMPROVE sampling location (Malm et al., 2004; Malm and Sisler, 2000; Malm et al., 1994). The remaining instrumentation was housed in several trailers located approximately 100 m from the IMPROVE sampling site. The trailers contained instruments for measuring aerosol physical, hygroscopic, chemical and optical properties, and were also used for analytical work on-site. An additional set of IMPROVE samplers and a filter sampling system (URG Inc., Chapel Hill, NC) (Lee et al., 2004) were located on a scaffold next to the instrument trailers. Malm et al. (2005) provide a detailed discussion of the measurement systems, intercomparisons between redundant

measurements, and findings with regard to aerosol properties.

Light absorbing carbon (LAC) was measured using a two-wavelength aethalometer ( $\lambda = 350$  and 880 nm; Magee Scientific, Berkeley, CA). LAC is operationally defined as the component of the aerosol carbon, which attenuates a light beam operating at the near IR 880 nm wavelength. The UV channel of the instrument is sensitive to certain strongly UV-absorbing organic compounds present in wood smoke, and thus a divergence between the readings from the two wavelength channels, after a wavelength-dependent correction, is indicative of a wood-smoke-impacted aerosol (Allen et al., 2004). Elevated aerosol water-soluble potassium ( $\text{K}^+$ ) concentrations have been used as indicators of fire emissions in a number of studies (Niemi et al., 2004; Khalil and Rasmussen, 2003; Hays et al., 2002; Andreae et al., 1988; Andreae, 1983). Potassium and other ionic species were measured by ion chromatography from samples collected on filters. The URG system consisted of a teflon primary collection filter with a nylon backup filter to collect nitrate escaping the primary filter. Two denuders were used to collect gas phase ammonia ( $\text{NH}_3$ ) and nitric acid ( $\text{HNO}_3$ ) concentrations (Lee et al., 2004) and an additional backup denuder was included to capture any ammonia volatilizing from particles collected on the teflon filter. Organic carbon concentrations were determined from  $\text{PM}_{2.5}$  (particulate mass of particles having aerodynamic diameters less than 2.5  $\mu\text{m}$ ) collected with quartz fiber filters, and then analyzed

with the thermal optical reflectance (TOR) method (Chow et al., 1993). Organic carbon concentrations were corrected for positive absorption artifacts using data from secondary filters collected at the routine Yosemite IMPROVE site during the study. The median value from the secondary filters was subtracted from the measured value on the primary filter. No corrections were made to account for possible negative artifacts arising from volatilization of collected organic particles. Dry aerosol size distributions were measured using three different instruments, which, taken together sampled the size range  $0.035 < D_p < 2.5 \mu\text{m}$ . A differential mobility particle sizer (DMPS; TSI 3081 Differential Mobility Analyzer with TSI 3010 Condensation Particle Counter, TSI Inc., Minneapolis, MN) classified particles by their physical size from 0.035 to  $0.85 \mu\text{m}$ . An optical particle counter (OPC; LASAIR 1003, Particle Measurement Systems, Boulder, CO) sized particles based on their optical size over the range of 0.1– $2 \mu\text{m}$ . An aerodynamic particle sizer (TSI 3320) sized particles based on their aerodynamic diameter from approximately 0.5 to  $20 \mu\text{m}$ . An iterative alignment method was used to merge the DMPS and OPC distributions and retrieve the particle refractive index (McMeeking et al., 2005a; Hand and Kreidenweis, 2002). Ambient light scattering coefficients were determined at 550 nm using an NGN-2 (Optec Inc., Lowell, MI) open-air nephelometer (Molenar, 1997).

Measurements of the aerosol light scattering coefficient, size distribution, and black carbon concentration were performed at BFRS using instruments similar to those employed in YNP (Table 1). The BFRS ( $38.87^\circ\text{N}$ ,  $120.67^\circ\text{W}$ , 1315 m elevation) is located 75 km ENE of Sacramento, California and 150 km NNW of Turtleback Dome, Yosemite (Fig. 2). The Blodgett Forest sampling site is located in an evenly aged ponderosa pine plantation, planted in 1990, located near the Blodgett Forest Research Station, owned by Sierra Pacific Industries. Aerosol size distributions for sizes ranging from 0.01 to  $0.4 \mu\text{m}$  were measured using a differential mobility particle spectrometer (DMPS) utilizing a differential mobility analyzer (TSI 3071A) coupled with a CPC (TSI 3760) as a detector. Light absorbing carbon concentrations were measured using a two-wavelength aethalometer (Magee Scientific, Berkeley, CA.) Ambient light scattering coefficients were measured at 550 nm using an NGN-2 open-air nephelometer. All instruments were located in individual enclosures mounted upon a 12 m walk-up tower. The air for the sample stream passed through a  $\text{PM}_{10}$  inlet followed by a  $\text{PM}_{2.5}$  sharp cut cyclone (Models 57-000596 and 57-005896, respec-

tively, Rupprecht & Patashnik Co. Inc., East Greenbush, NY), and all instruments except the nephelometer were isokinetically sampled from this stream. The inlet was mounted above the tower at a height of approximately 13 m. A more detailed description of the BFRS experimental setup is provided in Lunden et al. (2005).

The IMPROVE network monitors a number of aerosol properties, including  $\text{PM}_{2.5}$  and  $\text{PM}_{10}$ , ionic mass concentrations, including  $\text{SO}_4^{2-}$  and  $\text{NO}_3^-$ , and aerosol carbon and elemental mass concentrations. Aerosols are sampled through inlet cyclones onto a series of filters every third day from midnight to midnight the following day. Organic and elemental carbon mass concentrations in the  $\text{PM}_{2.5}$  fraction are determined using TOR, and corrected for absorption artifacts using medians from routinely-collected secondary filters at selected sites across the IMPROVE network; elemental species concentrations are determined by X-ray fluorescence (XRF) and particle induced X-ray emission (PIXE). Details regarding the network, measurement sites, monitoring protocols, and data reduction methods are given by Malm et al. (1994) and Malm et al. (2004). Data from 35 IMPROVE sites in Washington, Oregon, and California were used in this study; locations are shown in Fig. 2. A second IMPROVE sampler in YNP obtained daily (from roughly 08:00 local time to 08:00 the following day) data during the intensive study for comparison to other measurements conducted at Turtleback Dome, Yosemite.

Sun photometer data were obtained from the AERONET data network for two sites in the San Joaquin Valley operating during the study period. One instrument was located in Fresno, California ( $36.78^\circ\text{N}$ ,  $119.77^\circ\text{W}$ , 0 m elevation), approximately 100 km south of YNP, while the second was located in Corcoran, California ( $36.10^\circ\text{N}$ ,  $119.57^\circ\text{W}$ , 110 m elevation), 180 km SSE of YNP. Sun photometer data were cloud-screened and inverted to yield estimates of aerosol optical depth (column-integrated extinction coefficients) at multiple wavelengths and aerosol size distributions. Continuous dry light scattering coefficients were measured at the Fresno, California Particulate Matter Supersite ( $36.78^\circ\text{N}$ ,  $119.77^\circ\text{W}$ , 90 m elevation) using a heated nephelometer ( $\lambda = 530 \text{ nm}$ ; Model M903, Radiance Research, Seattle, WA). The site is located in an urban setting approximately 1 km north of the downtown commercial district.

## 2.2. Western United States fire activity

Emissions from wild fires are difficult to characterize due to the highly variable nature of such fires and the uncertainties in emission factors of various species,

which depend on fuel type and fire stage (flaming or smoldering). Techniques for identifying fire activity include analysis of satellite observations (Ito and Penner, 2004; Simon et al., 2004; Gregoire et al., 2003; Roy et al., 2002) and use of inventories based on reports from land management agencies and firefighters. The National Interagency Fire Center (NIFC; <http://www.nifc.gov>) compiles lists of major fires in the United States, which are defined by the NIFC as any fire burning an area greater than 200 ha. The total area burned in the United States in 2002, as reported by the NIFC, was over 2.8 million hectares, one of the largest burned acreages on record. The 1960–2002 annual average area burned ( $\pm 1$  standard deviation) was  $1.66 \pm 0.66$  million hectares according to the NIFC. Roughly 600,000 ha ( $\sim 20\%$  of the total U.S. burn area in 2002) burned in Oregon and California in 2002, with Oregon seeing largest fire in terms of burned area, in the last century.

We used the NIFC fire reports to determine periods of most intense fire activity in Washington, Oregon and California, and to identify the locations of major fires occurring in these states during the observation period. Locations of all NIFC-reported fires active during the period 15 July–5 September 2002 in Washington, Oregon, and California are shown in Fig. 2. Two fires, the Biscuit Fire in southwestern Oregon and the McNally Fire in southern California, burned over

40,000 ha each, making them the largest fires active in the region during the study period. Total fire sizes, reported as the cumulative area burned, are shown in Fig. 3 for these two major fires and for three other large fires that were active during the study. The McNally Fire was most active from 23 to 25 July 2002, reaching nearly half its final size in that short time period, before displaying slower growth throughout most of August. The Biscuit Fire had several periods of rapid growth from 28 July to 20 August, when its size reached roughly 200,000 ha, over three times that of any other fire in the region during the study period. Two relatively large fires in Oregon, the Tiller Fire and the Monument Fire, were characterized by steady growth in size from late-July through August.

The size, locations, and number of numerous smaller ( $<200$  ha) wildfires and controlled burns, which may have occurred during the study are difficult to determine with confidence due to the lack of consistent reporting. However, the National Park Service (NPS) reported all smaller fires that were active within the YNP boundaries during the study. In general, these fires lasted on the order of several days and typically burned less than 40 ha. The largest fire inside the park during the study period was the lightning-caused Wolf Complex fire, one mile west of White Wolf Lodge, which was allowed to burn slowly from its start on 11 July through most of August.

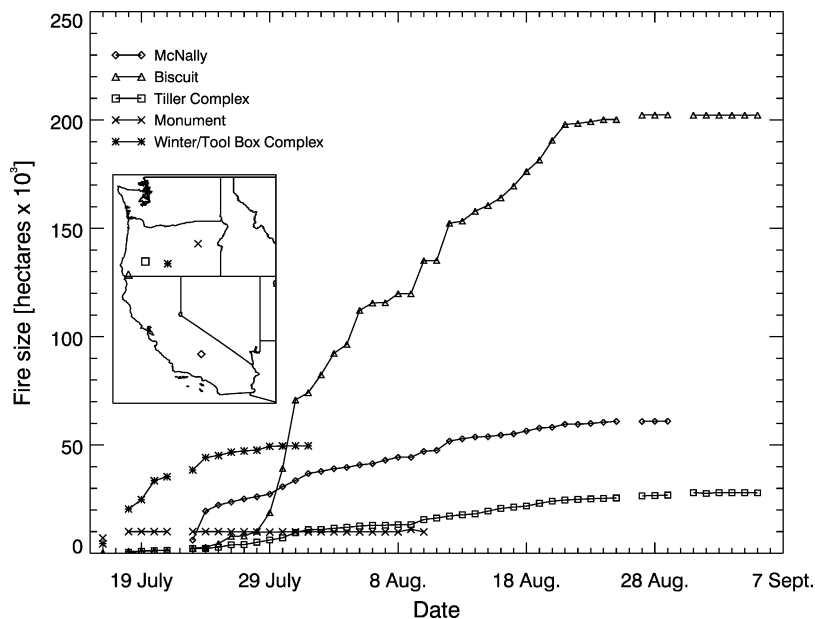


Fig. 3. Cumulative burn area (in thousands of hectares) for selected fires occurring during the summer of 2002 as reported by the National Interagency Fire Center.

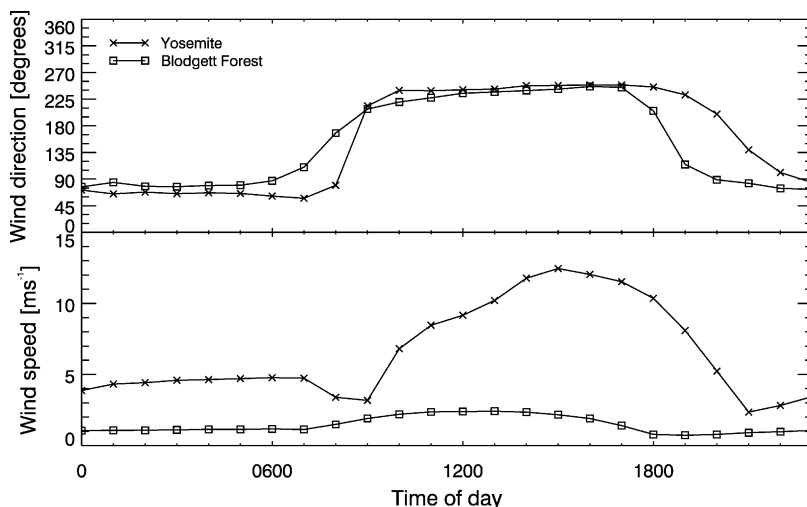


Fig. 4. Average diurnal wind speed and direction patterns observed at Yosemite National Park and at BFRS.

### 2.3. Meteorological conditions during the summer of 2002

Local transport at the YNP and BFRS measurement sites was characterized by a strong, thermally-driven mountain-valley wind circulation. Fig. 4 shows hourly-averaged wind speed and direction for each site. During the day, the sites are influenced by up-slope (westerly) flow, which brings San Joaquin Valley and Sacramento Valley air masses to the study sites. This pattern reverses during the night, with down-slope (easterly) winds occurring at both study locations. The shift between up- and down-slope flows occurred earlier at BFRS than at YNP due to the lower elevation of the BFRS site. The wind speeds at the YNP site are higher than those measured at the BFRS, probably due to the higher elevation and exposed nature of the elevated YNP site.

Large-scale transport patterns at BFRS and YNP were simulated using the NOAA Hybrid Single-Particle Lagrangian Integrated Trajectory (HYSPPLIT v 4.7) model (Draxler and Rolph, 2003; Rolph, 2003). The model was used to generate 5-day backward trajectories for arrival heights of 500 m above ground level for each site for every hour during the study period. The final analysis (FNL) data product of the Global Data Assimilation System (GDAS) with modeled vertical velocities was used to calculate the backward trajectories. These gridded data used the global spectral medium range forecast (MRF) model to assimilate multiple sources of measured data. The data were on a  $129 \times 129$  polar stereographic grid with 120 km resolution and 12 vertical layers on constant pressure surfaces from 1000 to 50 hPa (<http://www.ncep.noaa.gov>).

Backward trajectories were used to determine contribution functions for air parcels arriving at each measurement location (Ashbaugh et al., 1985). Contribution functions represent the relative contribution of transport from areas surrounding a location to that location. By defining the residence time in a grid cell as the number of backward trajectory endpoints contained within the cell over a specified time interval, the contribution function for that cell is determined from the residence time of the cell divided by the total number of trajectory endpoints during the specified time interval. Normalizing this quantity by the residence time expected for a hypothetical distribution of trajectories arriving at the site from all directions with equal probability gives a source contribution function, a non-dimensional, statistical metric for evaluating the significance of transport patterns.

Contour plots of source contribution function values greater than one, representing higher-than-random probability of an air parcel coming from that location, were constructed for YNP and BFRS for the entire study period (midnight, 15 July 2002–noon, 5 September 2002). The contours shown in Fig. 5 were color-scaled to indicate those regions over which air parcels spent the most time. Similar transport patterns can be seen for both study sites, with the majority of air parcels traveling over the Pacific Northwest and northern California before reaching the site, frequently passing through the San Francisco Bay and Sacramento Delta areas and then across the San Joaquin Valley. Comparison of Fig. 5 to the fire locations and activities shown in Figs. 2 and 3 suggests the majority of air parcels reaching Blodgett Forest and Yosemite traveled over areas in southwestern and south-central Oregon

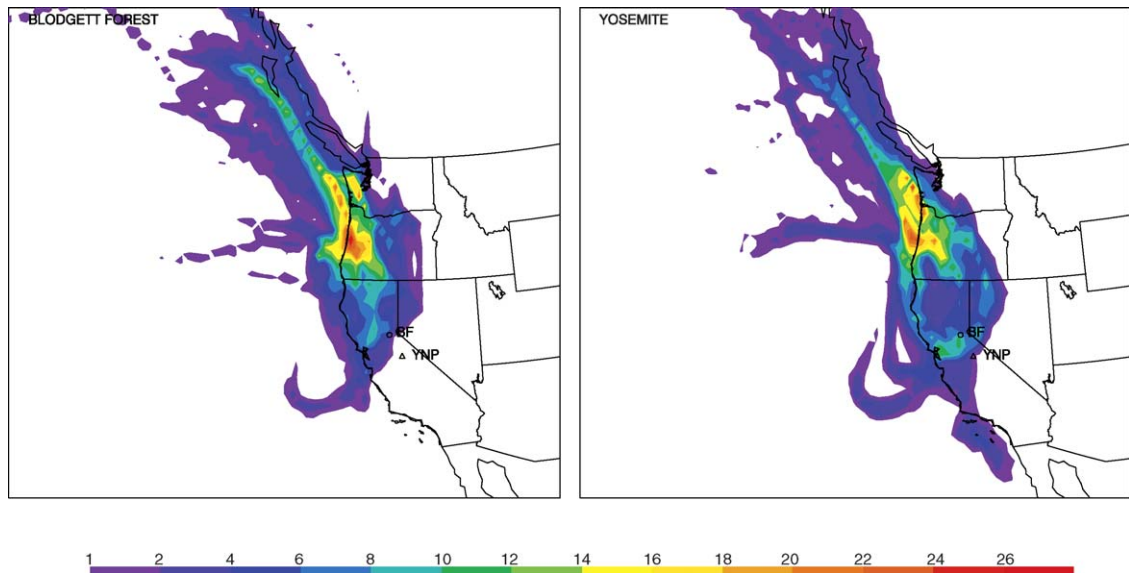


Fig. 5. Values of the non-dimensional source contribution function, a statistical metric used to analyze backward trajectories. The source contribution function was calculated from HYSPLIT backward trajectories with a 500 m above ground level arrival height during 15 July–5 September 2002 for Blodgett Forest (left panel) and Yosemite NP (right panel). Warmer colors indicate a higher probability of transport from a region to the specific measurement site.

with significant fire activity. In general, transport time from Oregon to the YNP and BFRS sites was 2–3 days. These results indicate likely transport of wildfire emissions to both BFRS and YNP. No backward trajectories indicated significant transport from the McNally Fire to YNP or BFRS, despite its closer proximity to the study locations. It is difficult to rule out influence from the McNally fire, however, due to the limitations of the modeled trajectories, particularly the coarseness of the model grid and velocity data when compared with the complex terrain of the region. If smoke from the McNally Fire was transported into the San Joaquin Valley, it could easily have been transported up the valleys in the western Sierra Nevada to both study sites by the strong thermally-driven wind systems.

### 3. Results and discussion

#### 3.1. Identification of smoke-impacted periods at YNP and BFRS

A number of similar measurements were made at BFRS and YNP including aethalometer measurements of LAC, nephelometer measurements of scattering coefficient ( $b_{sp}$ ), and size distribution measurements. Fig. 6a is a timeseries of hourly-averaged concentrations of LAC measured at BFRS and YNP. LAC concentrations are elevated and are similar in magnitude

at both sites from 8 to 20 August. We note this period is also that in which the Biscuit fire experienced rapid growth (Fig. 3) and large-scale transport suggested air masses from southwestern Oregon were arriving at both sites (Fig. 5). Despite the considerable distance between them, the overall variations in LAC are very similar at the two sites, although evidence for local effects is also seen. For example, two events with elevated LAC concentrations at BFRS but little change at YNP occurred near 17 and 27–28 July. However, the overall similar behavior of LAC concentrations at both sites suggests that observed haze was present on a regional scale, and that local sources of LAC were usually minimal relative to those acting on the larger scale.

The difference between the concentrations reported for UV and LAC channels ( $[UV] - [LAC]$ ), as measured by the aethalometers, is responsive to the presence of wood smoke and thus can be examined to indicate whether this source of LAC is important at the two sites. Timeseries of these data are shown in Fig. 6b. Occasionally both sites had episodically high values of  $[UV] - [LAC]$  at different times, but these 1–2 day events are superimposed on more dominant, similar general trends that again suggest broader-scale influence from fire activity in the region.

The data presented in Fig. 6 can be used to argue qualitatively for the influence of wood smoke on the haze observed at YNP and BFRS. Quantification of the

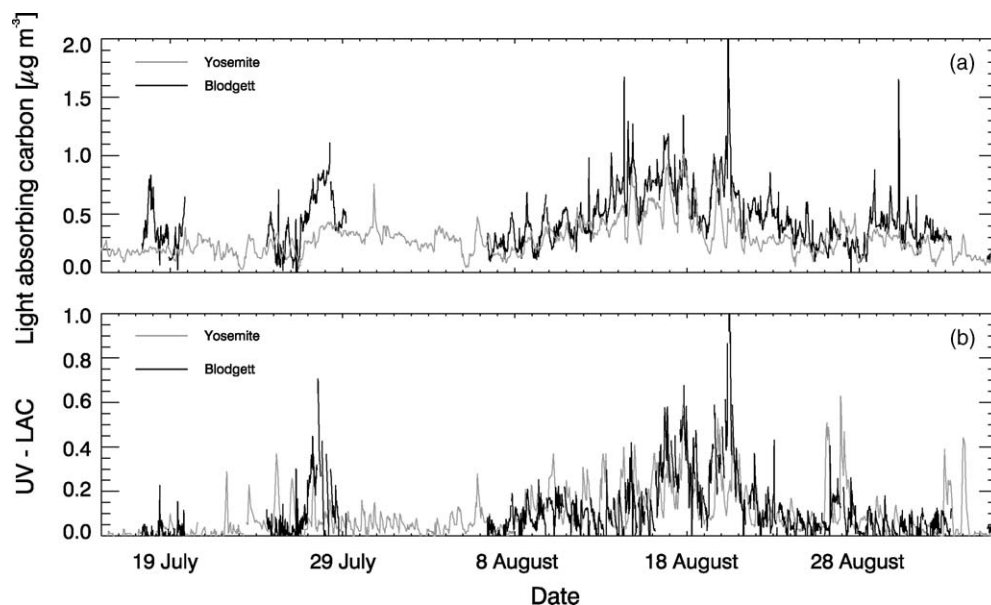


Fig. 6. Comparison of hourly-averaged (a) aethalometer light-absorbing carbon concentrations as measured in the visible channel and (b) the difference between mass concentrations in the ultraviolet channel [UV] and in the visible [LAC], measured at Turtleback Dome (Yosemite NP) and Blodgett Forest during the summer of 2002.

contribution of wood smoke to atmospheric particulate matter concentrations has typically been done using source apportionment methods such as positive matrix factorization (Henry et al., 1994), UNMIX (Paatero, 1997), and multivariate receptor modeling (Park et al., 2002). Estimates of wood smoke contributions in YNP during this study, using organic molecular markers and the wood smoke source profiles of Hays et al. (2002), have been reported by Engling et al. (2005). The estimated average daily contributions of primary fire emissions were as high as 65%. Here, we present a more qualitative assessment of fire impacts using data from the measurements summarized in Table 1.

Timeseries of the daily-averaged concentrations of several chemical smoke indicators measured at YNP are presented in Fig. 7. Several distinct periods of elevated URG-measured potassium ion concentrations, elevated [UV], and elevated aerosol OC concentration are evident in the timeseries, particularly in late July and mid-August. Fig. 7 also shows the timeseries of the ratio of fine particulate OC concentrations to elemental carbon (EC) concentrations measured at the IMPROVE site. This ratio has been used as a first approximation to distinguish primary emissions from mobile sources and industrial facilities from those due to vegetative fires (Malm et al., 2004). Values of  $\text{PM}_{2.5}$  OC and EC concentrations for YNP were taken from the IMPROVE measurements for comparison with other sites in the

network. The OC/EC ratios of emissions from vegetative fires tend to be much higher than those for mobile sources and industrial emissions (Gillies et al., 2001; McDonald et al., 2000). Formenti et al. (2003) observed OC/EC ratios ranging from approximately 9–16 in fresh smoke plumes and aged regional haze over southern Africa during the burning season. Malm et al. (2004) give annual averages for the organic carbon mass-to-light absorbing carbon ratio of 4–5 for urban regions in the IMPROVE network and 11–12 for the northwestern United States, an area with historically high wild fire activity. Table 2 gives the daily-averaged values of wood smoke indicators at YNP. Periods when backward trajectory analyses indicated transport from active fire regions are also indicated.

To distinguish between smoke-emissions-impacted and non-impacted time periods, we performed a simple statistical analysis. First, we defined background (non-smoke-impacted) values of the various aerosol indicators using the average value observed during the time period from 14 July through 19 July (designated as days P0 through P5 in Table 2), during which no major fires were burning in the region. Only LAC data were available for 14 July. A two-sample, one-tailed *t*-test was then used to determine if values of each indicator observed on other days of the study were significantly greater than this background level at a 95% confidence level. Critical values,  $x_c$ , of the various indicators were determined using:

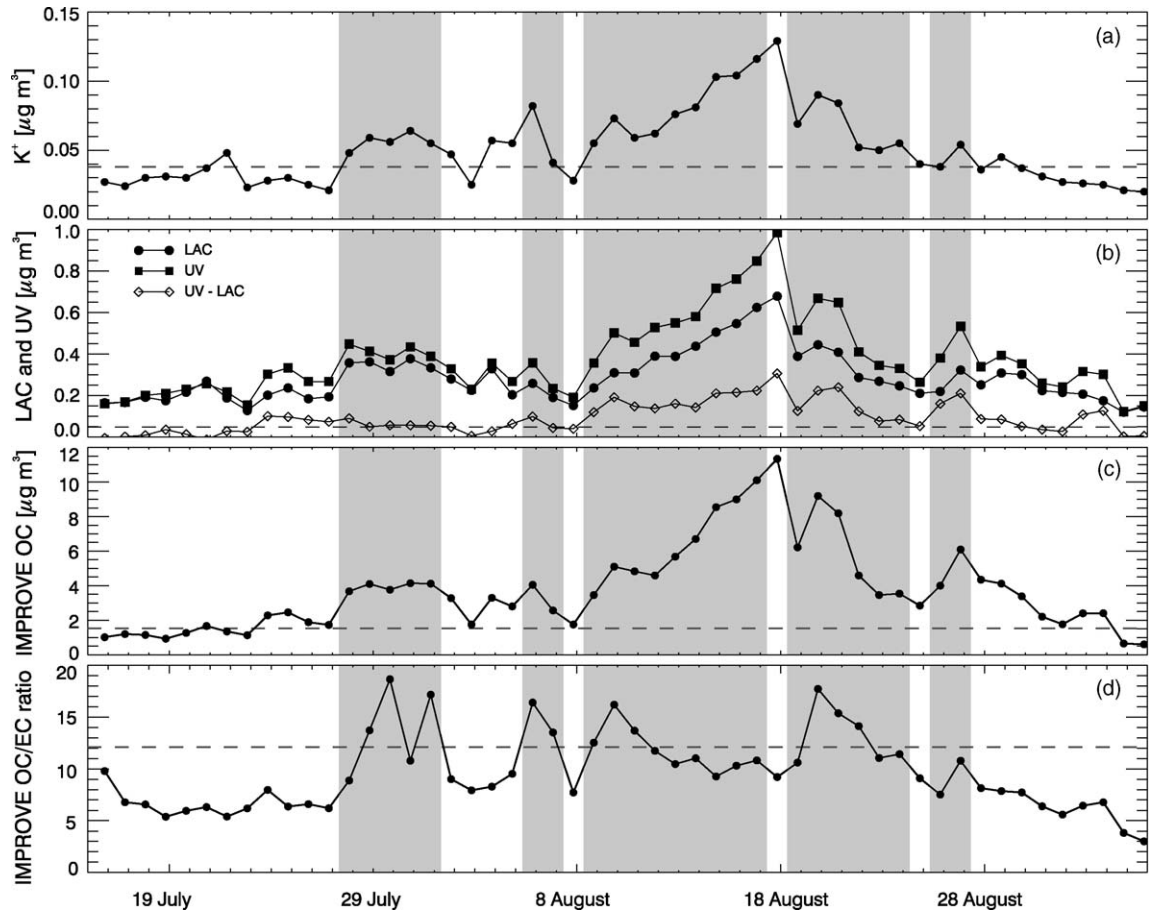


Fig. 7. Concentrations of  $\text{PM}_{2.5}$  potassium ion, IMPROVE organic/elemental carbon ratio and aethalometer-measured [LAC] and [UV] at Turtleback Dome in Yosemite National Park plotted at the midpoint of sample collection times (8 p.m.). Days passing at least four criteria, as compiled in Table 2, are shaded from 8 a.m. on the first impacted day to 8 a.m. on the first non-impacted day. Dashed lines indicate values of  $x_c$  determined from Eq. (1) for each species.

Table 2  
Daily values of smoke indicators at YNP (columns 3–8) and BFRS (columns 9–10)

Day of study	Date 8 a.m. to ~8 a.m.	$K^+$ ( $\mu\text{g m}^{-3}$ )	OC ( $\mu\text{g m}^{-3}$ ) IMPROVE $\text{PM}_{2.5}$	OC/EC IMPROVE $\text{PM}_{2.5}$	[UV] – [LAC]	Transport flag (Y = trajectory passed over fire); name of relevant fire; transport time to YNP (h)	Smoke-impact	[UV] – [LAC], BFRS	Smoke-impact, BFRS
$x_c$	–	0.038	1.529	12.10	0.048	–	–	0.04	
P0	7/14	–	–	–	0.00	N			
P1	7/15	0.027	1.02	9.8	0.00	N			
P2	7/16	0.024	1.20	6.8	0.00	N			
P3	7/17	0.030	1.15	6.6	0.01	N		–0.02	
P4	7/18	0.031	0.93	5.4	0.04	N		–0.01	
P5	7/19	0.030	1.27	6.0	0.01	N		0.00	
1	7/20	0.037	<b>1.67</b>	6.3	–0.01	N	●		
2	7/21	<b>0.048</b>	1.35	5.4	0.03	Y, Biscuit (60)	●●		
3	7/22	0.023	1.13	6.2	0.03	N			
4	7/23	0.028	<b>2.28</b>	8.0	<b>0.10</b>	N (stagnant)	●●		
5	7/24	0.030	<b>2.46</b>	6.4	<b>0.10</b>	Y, Fifty Eight (72)	●●●●	0.04	
6	7/25	0.025	<b>1.89</b>	6.6	<b>0.08</b>	N	●●	0.01	

Table 2 (Continued)

Day of study	Date 8 a.m. to ~8 a.m.	K <sup>+</sup> (μg m <sup>-3</sup> )	OC (μg m <sup>-3</sup> ) IMPROVE PM <sub>2.5</sub>	OC/EC IMPROVE PM <sub>2.5</sub>	[UV] – [LAC]	Transport flag (Y = trajectory passed over fire); name of relevant fire; transport time to YNP (h)	Smoke-impact	[UV] – [LAC], BFRS	Smoke-impact, BFRS
7	7/26	0.021	1.73	6.2	0.07	N	●●	0.05	●
8	7/27	0.048	3.68	8.9	0.09	Y, Tool Box (54), Winter, Grizzly (48)	●●●●	0.29	●
9	7/28	0.059	4.10	13.7	0.05	Y, Tiller (54), Skunk (48)	●●●●●	0.08	●
10	7/29	0.056	3.77	18.6	0.06	Y, Eyerly (60)	●●●●●	-0.05	
11	7/30	0.064	4.14	10.8	0.06	Y, Sheldon Ridge (72), White River (66)	●●●●		
12	7/31	0.055	4.12	17.2	0.05	Y, Tool Box (84)	●●●●●		
13	8/1	0.047	3.28	9.0	0.05	N	●●●		
14	8/2	0.025	1.75	7.9	0.01	N	●		
15	8/3	0.057	3.30	8.3	0.03	N	●●		
16	8/4	0.055	2.80	9.5	0.06	N	●●●		
17	8/5	0.082	4.05	16.4	0.10	N	●●●●		
18	8/6	0.041	2.57	13.5	0.04	Y, Biscuit (60)	●●●●	0.03	
19	8/7	0.028	1.75	7.7	0.04	Y, Biscuit (72)	●●	0.03	
20	8/8	0.055	3.46	12.5	0.12	Y, Tiller (108), Tool Box (72)	●●●●	0.09	●
21	8/9	0.073	5.10	16.2	0.19	Y, Tool Box (78)	●●●●●	0.09	●
22	8/10	0.059	4.83	13.7	0.15	Y, Tiller (90)	●●●●●	0.14	●
23	8/11	0.062	4.59	11.7	0.14	Y, Monument (102)	●●●●	0.09	●
24	8/12	0.076	5.68	10.5	0.16	Y, Monument (120)	●●●●	0.05	●
25	8/13	0.081	6.70	11.0	0.14	Y, Monument (66)	●●●●	0.05	●
26	8/14	0.103	8.54	9.3	0.21	Y, Monument (78)	●●●●	0.13	●
27	8/15	0.104	8.99	10.3	0.21	Y, Monument (78)	●●●●●	0.08	●
28	8/16	0.116	10.10	10.8	0.22	Y, Biscuit (120)	●●●●	0.29	●
29	8/17	0.129	11.34	9.2	0.31	N	●●●	0.37	●
30	8/18	0.069	6.21	10.6	0.13	Y, Biscuit (66)	●●●●	0.24	●
31	8/19	0.090	9.19	17.7	0.22	Y, Biscuit (60)	●●●●●	0.27	●
32	8/20	0.084	8.19	15.4	0.24	N	●●●●	0.52	●
33	8/21	0.052	4.59	14.1	0.12	N	●●●●	0.17	●
34	8/22	0.050	3.46	11.1	0.08	Y, Biscuit (72)	●●●●	0.09	●
35	8/23	0.055	3.54	11.4	0.08	Y, Biscuit (72)	●●●●	0.08	●
36	8/24	0.040	2.85	9.1	0.05	N	●●●	0.04	
37	8/25	0.038	4.0	7.5	0.16	Y, Biscuit (84)	●●●●	0.04	
38	8/26	0.054	6.09	10.8	0.21	Y, Tiller (66)	●●●●	0.12	●
39	8/27	0.036	4.35	8.1	0.09	N	●●	0.08	●
40	8/28	0.045	4.12	7.9	0.09	N	●●●	0.02	
41	8/29	0.037	3.38	7.7	0.05	N	●●	0.02	
42	8/30	0.031	2.20	6.4	0.04	Y, Tiller (84)	●●	0.00	
43	8/31	0.027	1.76	5.6	0.03	Y, Biscuit (114)	●●	0.02	
44	9/1	0.026	2.40	6.4	0.11	N	●●	0.04	●
45	9/2	0.025	2.41	6.8	0.13	N	●●	0.04	●
46	9/3	0.021	0.65	3.8	0.0	Y, Biscuit (90)	●		
47	9/4	0.020	0.60	3.0	0.01	Y, Biscuit (90)	●	0.03	

$$x_c = x + ts_1 \sqrt{\frac{n_1 + n_2}{n_1 n_2}} \quad (1)$$

where  $n_1$  is the number of background samples (5 or 6 for YNP),  $n_2$  is the number of test samples (1),  $s_1$  is the standard deviation of the background sample values,  $x$  is the sample mean determined from the background

samples, and  $t$  is the one-tailed  $t$ -statistic for 95% confidence and the appropriate degrees of freedom. The critical values computed for each indicator according to Eq. (1) are given in the first row of Table 2. If an observation during the period 20 July–4 September exceeds the critical value, then there is a statistically significant (95% confidence level) difference between the average non-smoke values and that day. Observations

meeting these criteria are indicated by bold-face text in Table 2. The transport criterion (transport flag = Y) was met if the backward trajectory arriving at noon on a given day had passed over an active fire region. The transport time from the fire region to the site in hours was determined using the HYSPLIT trajectories and is indicated in parentheses after the value of the transport flag. The number of dots in column 8 of Table 2, ranging from 0 to 5, denote the number of criteria that were met for YNP data on each day.

The strongest evidence for sustained fire impact at YNP occurred for the periods 27–31 July and 8–16 August, when four or five smoke indicators met the criteria for smoke-impact. With the exception of 17 August, four or five criteria were also met for the week following the August event, up to 23 August. The organic carbon criterion was met on the largest number of days, including days on which potassium or [UV] – [LAC] criteria were not met, reflecting the likely influence of increases in biogenic secondary organic aerosol across the region. In general, however, the combination of the five indicators presented in Table 2 appears to suggest that there were frequent impacts from fire emissions at the Yosemite site, particularly for the regional event occurring in mid-August.

Data for one of the indicators used at YNP, [UV] – [LAC], were also available for the BFRS site. We applied Eq. (1) to determine a critical value for BFRS based on three observations during the 15–19 July period, and in Table 2 show the dates when this criterion was exceeded. These include the extended period 8–23 August, consistent with the extended smoke-influenced period observed for YNP.

### 3.2. Spatial extent of haze

Concentrations of EC, OC, potassium in the  $PM_{2.5}$  aerosol fraction, and fine aerosol mass, as reported in the IMPROVE database, were used to determine the spatial extent of the haze across the states of Washington, Oregon, and California. Fig. 8 compares observed concentrations from a day with little wildfire activity (16 July 2002) to those measured on a day with much higher wildfire activity (18 August 2002). On 16 July only two large fires were active in this region, both in central Oregon.

The annual average concentrations measured by IMPROVE ( $\mu\text{g m}^{-3}$ ) from 1998 to 2004 at Turtleback Dome, Yosemite were  $1.71 \pm 2.95$  for OC,  $0.26 \pm 0.39$  for EC,  $0.04 \pm 0.03$  for potassium, and  $4.77 \pm 4.08$  for  $PM_{2.5}$ . These compare to the July 16 and August 18

measurements, respectively, of 1.7 and 9.1 for OC, 0.18 and 0.80 for EC, 0.014 and 0.108 for potassium, and 2.3 and 18.8 for  $PM_{2.5}$ . Concentrations of organic carbon, elemental carbon, and fine mass on 18 August over the region were higher than historical annual averages from IMPROVE as reported for 1996–1998 (e.g. annually averaged OC in California and Oregon ranged from 0.75 to  $2.5 \mu\text{g m}^{-3}$ ; 0.08 to  $0.50 \mu\text{g m}^{-3}$  for EC; 2 to 9 for  $PM_{2.5}$ ; <http://www.vista.cira.colostate.edu/views>).

Concentrations of all of the selected aerosol fire indicators were low at most IMPROVE sites on 16 July 2002. Higher fine mass, OC, and EC concentrations were observed at the Crater Lake NP and Hells Canyon sites (located in southeastern Oregon and western Idaho, respectively), which were likely impacted by the nearby Toolbox/Winter and Monument Fires, respectively (Fig. 3). Nearby IMPROVE network observations suggest that these fires did not have appreciable effects on haze levels at YNP and BFRS.

In contrast, concentrations of EC, OC, potassium, and fine mass were all substantially higher throughout much of southern Oregon and California on 18 August 2002. The Biscuit, Tiller, and McNally Fires were the largest active fires during this time (both much larger than the Toolbox/Winter and Monument Fires). Very high ( $\sim 50 \mu\text{g m}^{-3}$ ) concentrations of fine aerosol mass were observed at IMPROVE sites closest to active fires, such as Crater Lake NP and Sequoia NP (located in central eastern California south of YNP), although elevated concentrations were seen at the majority of sites throughout California. The highest concentrations of OC ( $> 80 \mu\text{g m}^{-3}$  in the 18 August sample) occurred at the Kalmiopsis Wilderness Area in southwestern Oregon, which is at an elevation of 90 m and was located very close to the large and active Biscuit Fire. Forward trajectories computed for this time period, beginning at the Biscuit Fire location, indicated northerly transport over Oregon and northern California, consistent with the IMPROVE observations of elevated haze throughout this region. Fig. 9 shows an example MODIS image for 16 August in which these smoke transport pathways are evident, particularly the offshore flow in SW OR that flows down the CA coast and back into the central CA valley via the San Francisco Bay and Sacramento Delta. At IMPROVE sites in western Oregon and the Sierra Nevada region (Kalmiopsis WA and Sequoia NP), the typical summertime concentrations of OC and  $PM_{2.5}$  are  $1\text{--}3 \mu\text{g m}^{-3}$  and  $5\text{--}15 \mu\text{g m}^{-3}$ , respectively. The widespread elevated mass concentrations of carbonaceous aerosol and fine particles evident on 18 August indicates that the wildfires active during this time had a

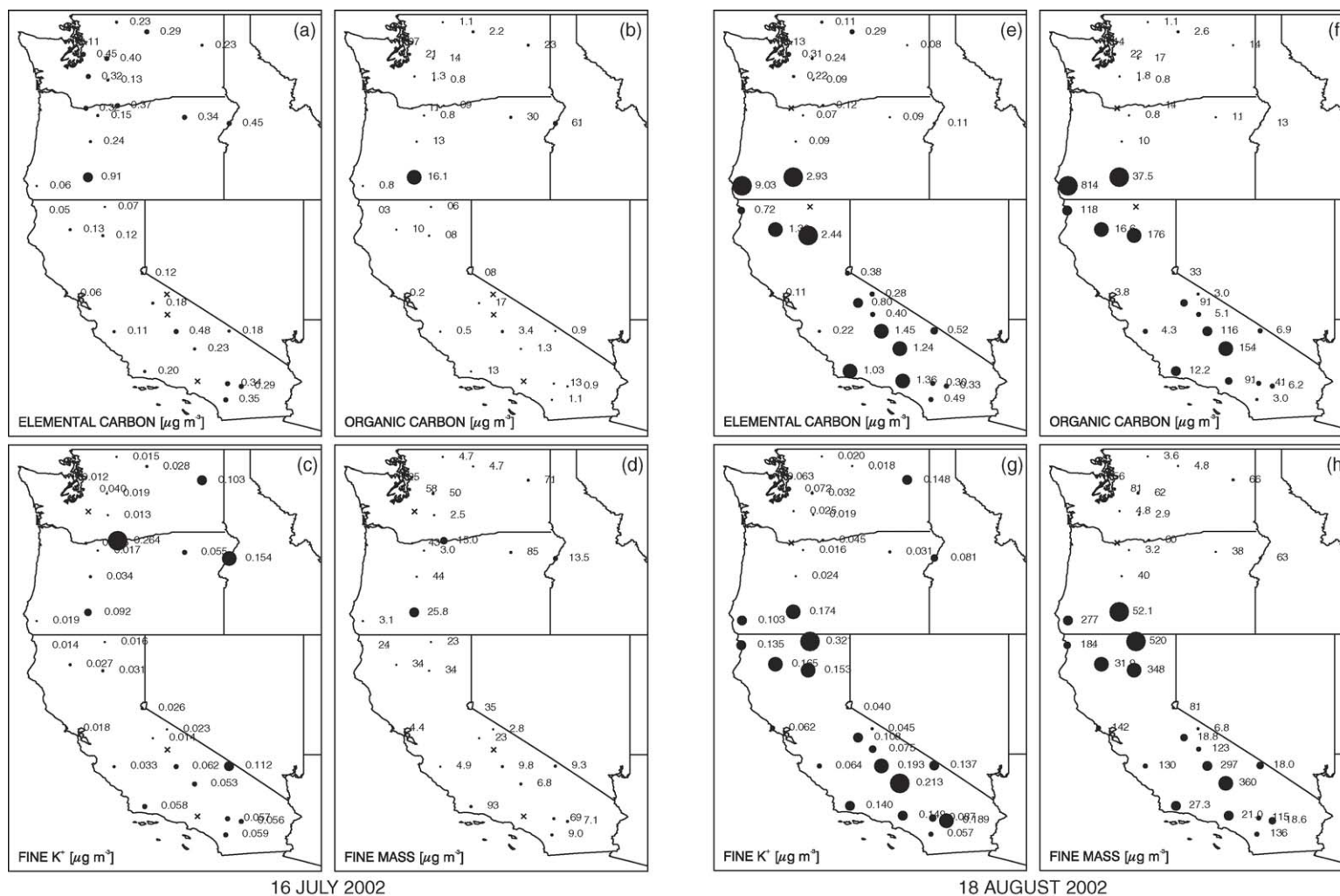


Fig. 8. Concentrations of elemental and organic carbon, potassium ion and  $\text{PM}_{2.5}$  gravimetric mass (all in  $\mu\text{g m}^{-3}$ ) observed by the IMPROVE network in Washington, Oregon, and California on 16 July 2002 (relatively clean) and 18 August 2002 (smoke-influenced).

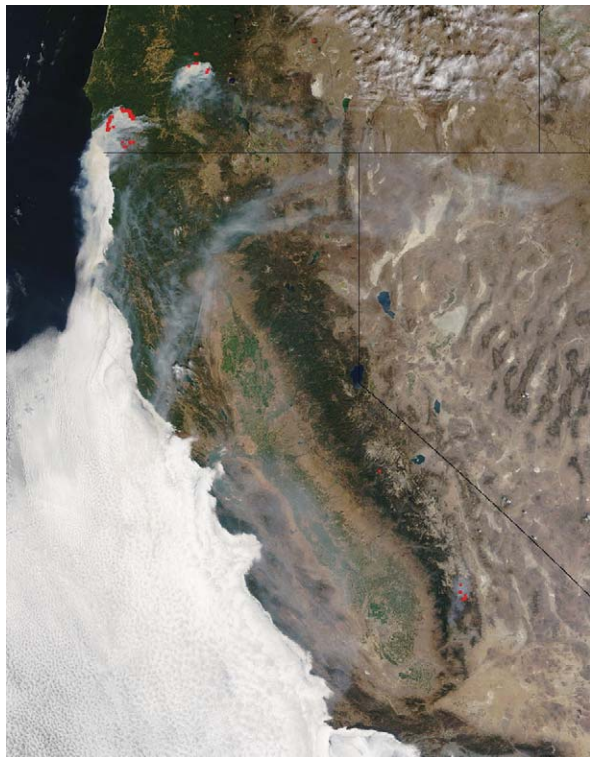


Fig. 9. MODIS image from 18 August (image courtesy of MODIS Rapid Response Project at NASA/GSFC).

regional-scale impact throughout the western United States, and likely dominated visibility degradation during several extended episodes during the summer of 2002.

Aerosol optical properties observed at several locations in and around California's central valley provide additional evidence of the regional-scale impact of these wildfires. Fig. 10 presents nephelometer measurements of the aerosol scattering coefficient ( $\lambda = 550, 550, 530$  nm, respectively),  $b_{sp}$ , at YNP, BFRS, and Fresno, and optical depth,  $\tau$ , at 670 nm determined by AERONET sun photometer measurements at the Fresno and Corcoran sites. Aerosol scattering coefficients and optical depths increase at all sites from approximately 27 July to 1 August and again from 8 August to 20 August. These time periods coincide with the independently-determined regional smoke-influenced haze episodes identified in Table 2. Other periods show weaker agreement between the aerosol measurements made at the elevated YNP and BFRS sites and the valley sites, such as the period 3–7 August and 26–31 August. The overall strong correlations between aerosol properties observed at these four sites suggests that wildfire smoke-impacted aerosol led to the increased optical depths and scattering coefficients.

Size distribution statistics (volume geometric mean diameter and standard deviation) were determined for

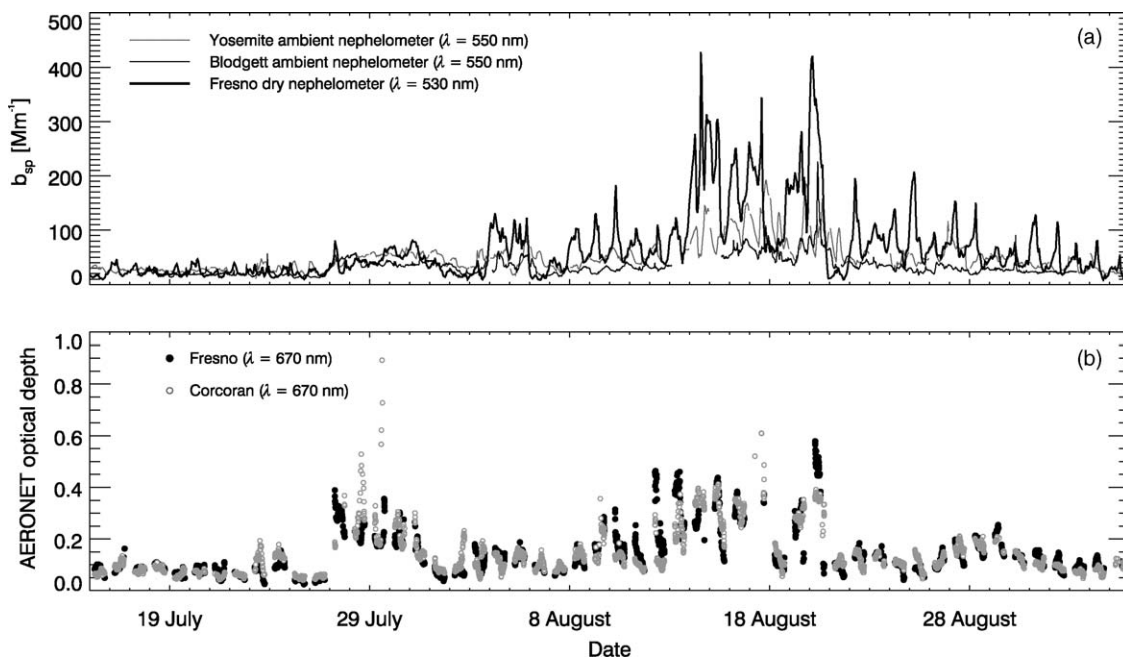


Fig. 10. Ambient aerosol scattering coefficients (a),  $b_{sp}$  ( $Mm^{-1}$ ), measured at Turtleback Dome (Yosemite NP) and Blodgett Forest during the summer of 2002. Both measurements were made using Optec NGN-2 open-air nephelometers operating at an effective wavelength of 550 nm. Also shown are nephelometer measurements ( $\lambda = 530$  nm) made at an urban San Joaquin Valley site (Fresno, California). Optical depths at  $\lambda = 670$  nm (b) are shown for two AERONET sites in the San Joaquin Valley operating during the study period.

size distributions measured at BFRS and YNP and for size distributions retrieved from sun photometer measurements at Fresno and Corcoran. Number geometric mean diameters were calculated for directly measured size distributions at YNP and BFRS using Eq. (2) (Hinds, 1999):

$$\log D_{gn} = \frac{\sum_{i=0}^n \log d_i n_i (\log D_p) d \log D_p}{N} \quad (2)$$

where  $n_i(\log D_p)$  is the value of the number distribution ( $dN/d\log D_p$ ,  $\text{cm}^{-3}$ ) in bin  $i$ ,  $d_i$  ( $\mu\text{m}$ ) is the geometric midpoint diameter of the bin,  $N$  is the total number concentration ( $\text{cm}^{-3}$ ), and  $n$  is the number of bins within the desired interval of the distribution. The AERONET database reports the volume geometric mean diameter for an assumed fine mode ranging from  $0.1 < D_p < 1.2 \mu\text{m}$ . An equation similar to Eq. (2) was

used to compute the volume geometric mean diameter for YNP size distributions, but for comparison with the AERONET data, limited to sizes in the accumulation mode (generally spanning the interval  $0.035\text{--}1 \mu\text{m}$ ) using the method given by McMeeking et al. (2005a).

Timeseries of number geometric mean diameters for YNP and BFRS, and for volume geometric mean diameters at YNP and both AERONET sites, showed remarkably good agreement, as seen in Fig. 11. Geometric mean diameters at all three sites increased during smoke-impacted episodes. This increase in geometric mean diameter has been noted in aged biomass burning-influenced hazes (Reid et al., 2005). Volume geometric mean diameters observed at YNP and at the AERONET sites are in agreement with published values given in a recent review by Reid et al. (2005).

Though the McNally fire was closer to the study sites than fires in Oregon, it did not appear to affect visibility

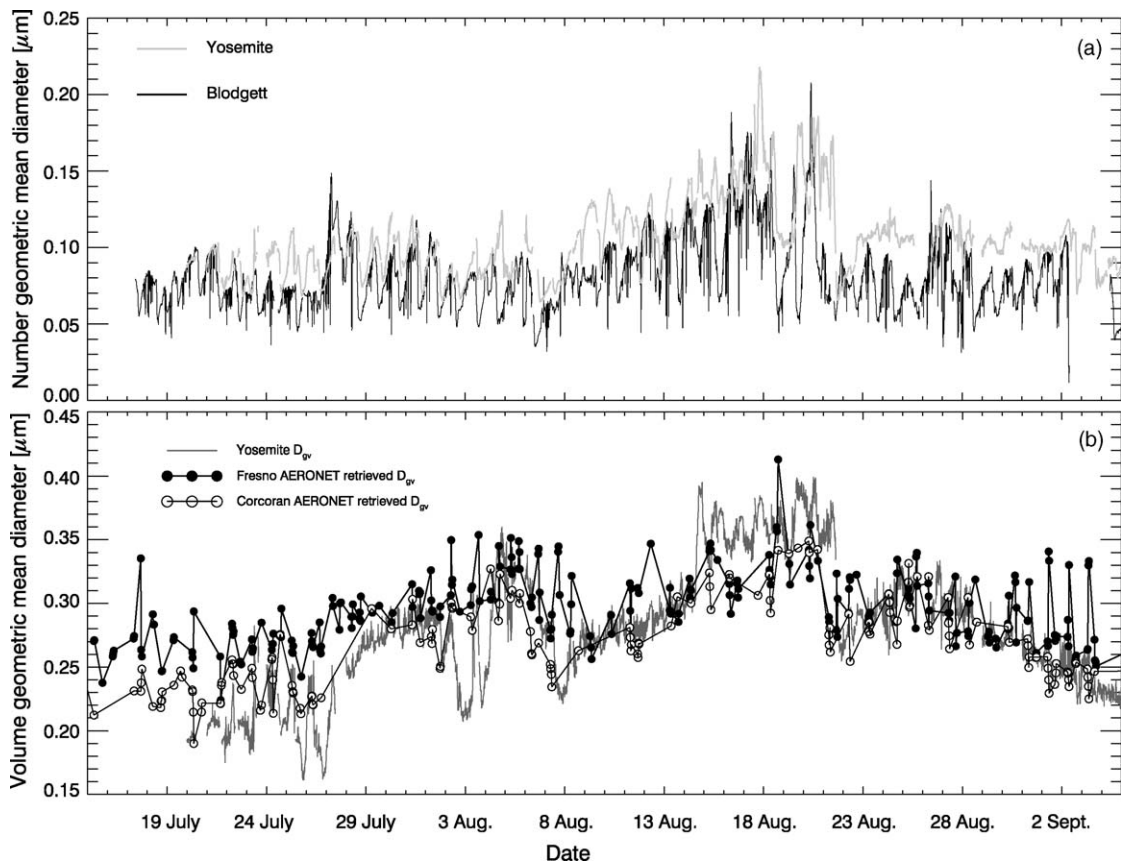


Fig. 11. (a) Timeseries of number geometric mean diameters ( $\mu\text{m}$ ) calculated from size distributions measured at Turtleback Dome (Yosemite NP) and Blodgett Forest using differential mobility analyzer and optical particle counter measurements. (b) Timeseries of volume geometric mean diameters from size distributions measured at YNP and retrieved from sun photometer measurements made by the AERONET network in Fresno, CA and Corcoran, CA during the summer of 2002. Uncertainties for Yosemite data were on the order of 1% and were due primarily to uncertainties in measured instrument flow rates. Dubovik et al. (2000) report uncertainties of approximately 25% for biomass burning aerosol for AERONET retrieved size distributions.

as strongly. Backward trajectory analyses indicated that there was little transport from the McNally fire to either YNP or BFRS. Furthermore, periods displaying the largest signals of wildfire smoke-impact, such as elevated potassium, UV absorption, and OC concentrations, occurred in mid-August. During this time the Biscuit Fire grew from roughly  $1.2 \times 10^5$  ha to nearly  $1.6 \times 10^5$  ha while the McNally Fire cumulative burn area only increased by approximately  $0.1 \times 10^5$  ha. The period of the McNally Fire's most rapid growth, and presumably greatest emissions, occurred roughly from 23 to 25 July. Smoke indicators did increase during this time, but not as much as they did during the mid-August event. The McNally Fire may have had a stronger influence on the San Joaquin Valley, as optical depths observed in Fresno and Corcoran during late-July were only slightly lower than those seen during the mid-August episode. As mentioned previously, this also suggests at least some influence on YNP and BFRS aerosols, because thermally-driven winds regularly transported San Joaquin Valley air to those sites.

#### 4. Conclusions

We have presented measurements of aerosol properties at a number of locations in California, Oregon, and Washington during 15 July–5 September 2002, a period of high wildland fire activity in this region. Two of the sites had continuous, high-time-resolution data for aerosol light scattering coefficients, black carbon concentrations, and aerosol size distributions. Variations in these quantities followed similar patterns at both study sites, indicating that the particles sampled in each location were likely influenced by similar regional-scale sources. IMPROVE network data from the region indicate elevated aerosol concentrations for a large number of wilderness areas and national parks throughout the region during this time period. These data also suggest an influence from wildfire emissions, deduced from elevated levels of aerosol organic carbon and soluble potassium. Fire emissions contributed to regional haze for prolonged, in some cases week-long, time periods. McMeeking et al. (2005a) showed that smoke-impacted aerosols observed at Yosemite NP during this period were highly effective at scattering visible light. This finding, combined with the regional-scale nature of wildfire-impacted aerosols reported here, suggests that wildfire emissions have a strong impact on visibility in a large number of Class I areas, even those located hundreds of miles from the fire activity.

Additional observations confirm the regional nature of this impact. Observations of aerosol properties at two

San Joaquin Valley sites were shown to be in close agreement with and to have temporal variations similar to aerosol measurements at Yosemite NP, indicating that these urban and semi-urban regions were also impacted by wildfire emissions. Thus wildfire activity may negatively impact the typically poor summertime air quality in these regions.

#### Acknowledgements

We thank Air Resource Specialists and Yosemite National Park staff for their assistance during the field study and the National Interagency Fire Center and K. Warner for national and park fire activity data. The authors gratefully acknowledge the NOAA Air Resources Laboratory (ARL) for the provision of the HYSPLIT transport and dispersion model and READY website (<http://www.arl.noaa.gov/ready.html>) used in this publication. Data provided from AERONET #102 Fresno, California and #59 Corcoran, California are courtesy of the Multiangle Imaging SpectroRadiometer (MISR) project, in affiliation with the Jet Propulsion Laboratory, California Institute of Technology, and under contract with the National Aeronautics and Space Administration. We acknowledge the AERONET project staff at Goddard Space Flight Center for making data available. We thank the MODIS Rapid Response Project at NASA/GSFC for the MODIS image. The Fresno Supersite nephelometer data was retrieved March 2005 from the Central California Air Quality Studies' (CCAQS) website (<http://www.arb.ca.gov/airways/>). Fresno Supersite data were collected as part of US Environmental Protection Agency (EPA) Assistance Agreement No. R-82805701-01. Support for Yosemite NP work was provided by the National Park Service (contract #CA2380-99001 TO0356). Work at the Blodgett Forest Research Site was supported by the Assistant Secretary for Fossil Energy, Office of Natural Gas and Petroleum Technology, through the National Petroleum Technology Office under U.S. Department of Energy Contract No. DE-AC03-76SF00098 and the Independent Petroleum Association of Mountain States. We would like to acknowledge Bob Heald and the Blodgett Forest crew for operational support. Kristi Gebhart assisted with backward trajectory analyses.

#### References

- Allen, G.A., Babich, P., Poirot, R.L., 2004. Evaluation of a new approach for real time assessment of wood smoke PM. In: *Regional and Global Perspectives on Haze: Causes, Consequences and Controversies—Visibility Specialty Conference*, Air and Waste Management Association, Asheville, North Carolina.

- Ames, R.B., Fox, D.G., Malm, W.C., Schichtel, B.A., 2004. Preliminary apportionments of carbonaceous aerosols to wild fire smoke using observations from the IMPROVE network. In: *Regional and Global Perspectives on Haze: Causes, Consequences and Controversies—Visibility Specialty Conference, Air and Waste Management Association, Asheville, North Carolina*.
- Andreae, M.O., 1983. Soot carbon and excess fine potassium—long-range transport of combustion-derived aerosols. *Science* 220, 1148–1151.
- Andreae, M.O., Brown, E.V., Garstang, M., Gregory, G.L., Harriss, R.C., Hill, G.F., Jacob, D.J., Pereira, M.C., Sachse, G.W., Setzer, A.W., Dias, P.L.S., Talbot, R.W., Torres, A.L., Wofsy, S.C., 1988. Biomass-burning emissions and associated haze layers over Amazonia. *J. Geophys. Res. Atmos.* 93, 1509–1527.
- Artaxo, P., Storms, H., Bruynseels, F., Vangrieken, R., Maenhaut, W., 1988. Composition and sources of aerosols from the Amazon basin. *J. Geophys. Res. Atmos.* 93, 1605–1615.
- Ashbaugh, L.L., Malm, W.C., Sadeh, W.Z., 1985. A residence time probability analysis of sulfur concentrations at Grand Canyon National Park. *Atmos. Environ.* 19, 1263–1270.
- Bench, G., Herckes, P., 2004. Measurement of contemporary and fossil carbon contents of PM<sub>2.5</sub> aerosols: results from Turtleback Dome, Yosemite National Park. *Environ. Sci. Technol.* 38, 2424–2427.
- Bevington, P.R., Robinson, D.K., 1992. *Data Reduction and Error Analysis for the Physical Sciences*. McGraw-Hill Inc., New York.
- Bond, T.C., Streets, D.G., Yarber, K.F., Nelso, S.M., Woo, J.-H., Klimont, Z., 2004. A technology-based global inventory of black and organic carbon emissions from combustion. *J. Geophys. Res.* 109, D14203, doi:10.1029/2003JD003697.
- Cachier, H., Lioussé, C., Buatmenard, P., Gaudichet, A., 1995. Particulate content of savanna fire emissions. *J. Atmos. Chem.* 22, 123–148.
- Carrico, C.M., Kreidenweis, S.M., Malm, W.C., Day, D.E., Lee, T., Carrillo, J., McMeeking, G.R., Collett Jr., J.L., 2005. Hygroscopic growth behavior of a carbon-dominated aerosol in Yosemite National Park. *Atmos. Environ.* 39, 1393–1404.
- Chow, J.C., Watson, J.G., Pritchett, L.C., Pierson, W.R., Frazier, C.A., Purcell, R.G., 1993. The DRI thermal optical reflectance carbon analysis system—description, evaluation and applications in United States air quality studies. *Atmos. Environ.* 27, 1185–1201.
- Draxler, R.R., Rolph, G.D., 2003. HYSPLIT (Hybrid Single-Particle Lagrangian Integrated Trajectory) model access via NOAA ARL READY, NOAA Air Resources Laboratory, Silver Spring, MD, website (<http://www.arl.noaa.gov/ready/hysplit4.html>).
- Dubovik, O., Smirnov, A., Holben, B.N., King, M.D., Kaufman, Y.J., Eck, T.F., Slutsker, I., 2000. Accuracy assessments of aerosol optical properties retrieved from Aerosol Robotic Network (AERONET) Sun and sky radiance measurements. *J. Geophys. Res. Atmos.* 105, 9791–9806.
- Engling, G., Herckes, P., Kreidenweis, S.M., Malm, W.C., Collett Jr. J.L., 2005. Composition of the fine organic aerosol in Yosemite National Park during the 2002 Yosemite Aerosol Characterization Study. *Atmos. Environ.*, in press.
- Formenti, P., Elbert, W., Maenhaut, W., Haywood, J., Osborne, S., Andreae, M.O., 2003. Inorganic and carbonaceous aerosols during the Southern African Regional Science Initiative (SAFARI 2000) experiment: chemical characteristics, physical properties, and emission data for smoke from African biomass burning. *J. Geophys. Res. Atmos.* 108, doi:10.1029/2002JD002408.
- Gillies, J.A., Gertler, A.W., Sagebiel, J.C., Dippel, W.A., 2001. On-road particulate matter (PM<sub>2.5</sub> and PM<sub>10</sub>) emissions in the Sepulveda Tunnel, Los Angeles, California. *Environ. Sci. Technol.* 35, 1054–1063.
- Gregoire, J.M., Tansey, K., Silva, J.M.N., 2003. The GBA2000 initiative: developing a global burnt area database from SPOT-VEGETATION imagery. *Int. J. Remote Sens.* 24, 1369–1376.
- Hand, J.L., Kreidenweis, S.M., 2002. A new method for retrieving particle refractive index and effective density from aerosol size distribution data. *Aerosol Sci. Technol.* 36, 1012–1026.
- Hand, J.L., Malm, W.C., Laskin, A., Day, D., Lee, T., Wang, C., Carrico, C., Carrillo, J., Cowin, J.P., Collett, J., Iedema, M.J., 2005. Optical, physical, and chemical properties of tar balls observed during the Yosemite Aerosol Characterization Study. *J. Geophys. Res. Atmos.* 110, doi:10.1029/2004JD005728.
- Hays, M.D., Geron, C.D., Linna, K.J., Smith, N.D., Schauer, J.J., 2002. Speciation of gas-phase and fine particle emissions from burning of foliar fuels. *Environ. Sci. Technol.* 36, 2281–2295.
- Henry, R.C., Lewis, C.W., Collins, J.F., 1994. Vehicle-related hydrocarbon source compositions from ambient data: the Grace-Safer method. *Environ. Sci. Technol.* 28, 823–832.
- Hinds, W.C., 1999. *Aerosol Technology*. Wiley, New York.
- Holben, B.N., Eck, T.F., Slutsker, I., Tanre, D., Buis, J.P., Setzer, A., Vermote, E., Reagan, J.A., Kaufman, Y.J., Nakajima, T., Lavenue, F., Jankowiak, I., Smirnov, A., 1998. AERONET—a federated instrument network and data archive for aerosol characterization. *Remote Sens. Environ.* 66, 1–16.
- Ito, A., Penner, J.E., 2004. Global estimates of biomass burning emissions based on satellite imagery for the year 2000. *J. Geophys. Res. Atmos.* 109, doi:10.1029/2003JD004423.
- Khalil, M.A.K., Rasmussen, R.A., 2003. Tracers of wood smoke. *Atmos. Environ.* 37, 1211–1222.
- Lee, T., Kreidenweis, S.M., Collett, J.L., 2004. Aerosol ion characteristics during the Big Bend Regional Aerosol and visibility observational study. *J. Air Waste Manage.* 54, 585–592.
- Lunden, M.M., Black, D.R., McKay, M., Revzan, K.L., Boldstein, A.H., Brown, N.J., 2005. Characteristics of fine particle growth events observed above a forested ecosystem in the Sierra Nevada Mountains of California. *Aerosol Sci. Technol.*, submitted for publication.
- Malm, W.C., Sisler, J.F., 2000. Spatial patterns of major aerosol species and selected heavy metals in the United States. *Fuel Process. Technol.* 65, 473–501.
- Malm, W.C., Sisler, J.F., Huffman, D., Eldred, R.A., Cahill, T.A., 1994. Spatial and seasonal trends in particle concentration and optical extinction in the United States. *J. Geophys. Res. Atmos.* 99, 1347–1370.
- Malm, W.C., Schichtel, B.A., Pitchford, M.L., Ashbaugh, L.L., Eldred, R.A., 2004. Spatial and monthly trends in speciated fine particle concentration in the United States. *J. Geophys. Res. Atmos.* 109.
- Malm, W.C., Day, D.E., Carrico, C., Kreidenweis, S.M., Collett Jr., J.L., McMeeking, G., Lee, T., Carrillo, J., 2005. Intercomparison and closure calculations using measurements of aerosol species and optical properties during the Yosemite Aerosol Characterization Study. *J. Geophys. Res.* 110, doi:10.1029/2004JD005494.
- McDonald, R.D., Zielinska, B., Fujita, E.M., Sagebiel, J.C., Chow, J.C., Watson, J.G., 2000. Fine particle and gaseous emission rates from residential wood combustion. *Environ. Sci. Technol.* 34, 2080–2091.
- McMeeking, G.R., Kreidenweis, S.M., Carrico, C.M., Lee, T., Collett, J.L., Malm, W.C., 2005a. Observations of smoke-influenced aerosol during the Yosemite Aerosol Characterization Study: size

- distributions and chemical composition. *J. Geophys. Res.* 110, doi:10.1029/2004JD005389.
- McMeeking, G.R., Kreidenweis, S.M., Carrico, C.M., Collett Jr., J.L., Day, D.E., Malm, W.C., 2005b. Observations of smoke-influenced aerosol during the Yosemite Aerosol Characterization Study. Part 2. Aerosol scattering and absorbing properties. *J. Geophys. Res.* 110, doi:10.1029/2004JD005624.
- Molenaar, J.V., 1997. Analysis of the real world performance of the Optec NGN-2 ambient nephelometers. In: *Visual Air Quality: Aerosols and Global Radiation Balance, Air and Waste Management Association, Pittsburgh*, pp. 243–265.
- Niemi, J.V., Tervahattu, H., Vehkamäki, H., Kulmala, M., Koskentalo, T., Sillanpää, M., Rantamäki, M., 2004. Characterization and source identification of a fine particle episode in Finland. *Atmos. Environ.* 38, 5003–5012.
- Niemi, J.V., Tervahattu, H., Vehkamäki, H., Martikainen, J., Laakso, L., Kulmala, M., Aarnio, P., Koskentalo, T., Sillanpää, M., Makkonen, U., 2005. Characterization of aerosol particle episodes in Finland caused by wildfires in Eastern Europe. *Atmos. Chem. Phys.* 5, 2299–2310.
- Paatero, P., 1997. A weighted non-negative least squares algorithm for three-way 'PARAFAC' factor analysis. *Chemometr. Intell. Lab.* 38, 223–242.
- Park, E.S., Oh, M.S., Guttorp, P., 2002. Multivariate receptor models and model uncertainty. *Chemometr. Intell. Lab.* 60, 49–67.
- Putaud, J.P., Raes, F., Van Dingenen, R., Brüggemann, E., Facchini, M.C., Decesari, S., Fuzzi, S., Gehrig, R., Hüglin, C., Laj, P., Lorbeer, G., Maenhaut, W., Mihalopoulos, N., Müller, K., Querol, X., Rodriguez, S., Schneider, J., Spindler, G., ten Brink, H., Torseth, K., Wiedensohler, A., 2004. European aerosol phenomenology-2: chemical characteristics of particulate matter at kerbside, urban, rural and background sites in Europe. *Atmos. Environ.* 38, 2579–2595.
- Reid, J.S., Koppmann, R., Eck, T.F., Eleuterio, D.P., 2005. A review of biomass burning emissions. Part II. Intensive physical properties of biomass burning particles. *Atmos. Chem. Phys.* 5, 799–825.
- Rogge, W.F., Mazurek, M.A., Hildemann, L.M., Cass, G.R., Simoneit, B.R.T., 1993. Quantification of urban organic aerosols at a molecular level: identification, abundance and seasonal variation. *Atmos. Environ.* 27, 1309–1330.
- Rolph, G.D., 2003. Real-time Environmental Applications and Display System (READY), NOAA Air Resources Laboratory, Silver Spring, MD, website (<http://www.arl.noaa.gov/ready/hysplit4.html>).
- Roy, D.P., Lewis, P.E., Justice, C.O., 2002. Burned area mapping using multi-temporal moderate spatial resolution data: a bi-directional reflectance model-based expectation approach. *Remote Sens. Environ.* 83, 263–286.
- Saxena, P., Hildemann, L.M., 1996. Water-soluble organics in atmospheric particles: a critical review of the literature and application of thermodynamics to identify candidate compounds. *J. Atmos. Chem.* 24, 57–109.
- Simon, M., Plummer, S., Fierens, F., Hoelzemann, J.J., Arino, O., 2004. Burnt area detection at global scale using ATSR-2: the GLOBSCAR products and their qualification. *J. Geophys. Res.* Atmos. 109, doi:10.1029/2003JD003622.
- Watson, J.G., 2002. Visibility: Science and regulation. *J. Air Waste Manage. Assoc.* 52, 628–713.